



LAWRENCE
LIVERMORE
NATIONAL
LABORATORY

Materials Characterization of Irradiated Spectralon from the NIF Target Chamber

R. Chow, G. Frieders, W. Jensen, M. Pearson, P.
Datte

May 22, 2015

Optical Engineering and Applications
San Diego, CA, United States
August 9, 2015 through August 13, 2015

Disclaimer

This document was prepared as an account of work sponsored by an agency of the United States government. Neither the United States government nor Lawrence Livermore National Security, LLC, nor any of their employees makes any warranty, expressed or implied, or assumes any legal liability or responsibility for the accuracy, completeness, or usefulness of any information, apparatus, product, or process disclosed, or represents that its use would not infringe privately owned rights. Reference herein to any specific commercial product, process, or service by trade name, trademark, manufacturer, or otherwise does not necessarily constitute or imply its endorsement, recommendation, or favoring by the United States government or Lawrence Livermore National Security, LLC. The views and opinions of authors expressed herein do not necessarily state or reflect those of the United States government or Lawrence Livermore National Security, LLC, and shall not be used for advertising or product endorsement purposes.

Materials Characterization of Irradiated Spectralon from the NIF Target Chamber

Robert Chow*, Gene Frieders, Wayne Jensen, Mark Pearson and Phil Datte

Affiliation: LLNL, 7000 East Ave., Livermore, CA, 94550, USA

Abstract

The Near Backscatter Imager (NBI) participates in nearly every kind of experiment conducted at NIF and measures backscatter, the result of the interaction between incident laser light and plasma waves at a target. Large Spectralon plates, on the order of a hundreds of mm per side, are used as Lambertian scatter components for the NBI diagnostics. The plates were deployed in 2009 and replaced in April of 2014. All NBI assemblies suffered reflectivity degradation, and some of these changes were spatially localized defects observed after irradiation to a cumulative combined neutron and γ dose of 0.038 Gy. The growth of a defect was correlated to the combined cumulative neutron and γ radiation dose from NIF fusion shots.

Spectralon plates that were irradiated to cumulative combined neutron and γ dose of 0.74 Gy were characterized for materials and mechanical changes with the following techniques: RBS, FTIR, XPS, SEM, EDX and tensile tests. These tests indicate that the bulk Spectralon did not measurably degrade but there are discolorations that affect the reflectivity. Surface analysis indicates that the surface CF_2 species re-forms to make various organic and CF_x species.

Keywords: National Ignition Facility, NIF, Spectralon, neutrons, gamma, radiation

1. INTRODUCTION

The LLNL Target Diagnostics community has to ensure the survivability and operability of materials used in the harsh radiation and energetic particle environment of the NIF target chamber¹. On one of these diagnostics, the Near Backscatter Imager (NBI), the irradiated sub-assemblies were extracted from the NIF target chamber during a planned upgrade. The material quality of the Spectralon exposed in such an environment was characterized. Developed in the mid-2000s, the NBI diagnostic is run during nearly every kind of experiment conducted at NIF and measures backscatter, the result of the interaction between incident laser light and plasma waves at a target suspended within a holraum^{2,3}.

Plasmas are composed on free ions and free electrons. Both the ions and electrons can have high amplitude waves. When the laser interacts with ion waves, the resultant scattered light is called Stimulated Brillouin Backscattering (SBS). The SBS backscattered light is close to the incident light wavelength and returns back into the laser beam lines, where, if not controlled, it can reach powers and energies sufficient to damage optics in the NIF laser system.

Electrons produce high frequency waves in the plasma. Light scatter from the electron plasma waves is called Stimulated Raman Backscattering (SRS), a type of laser-plasma instability. In SRS, electron density fluctuations in the plasma cause the incident laser light to scatter resonantly. High levels of backscatter reduce the coupling of laser energy to the fusion target and constrain implosion symmetry and other design parameters.

NBI provides an accurate total SBS and SRS backscattered energy measurements on the NIF. The diagnostic does this by measuring the light backscattered outside the NIF beam lines onto Spectralon scatter plate assemblies surrounding specific beam quads. Precisely calibrated images of the backscattered light on the scatter plates are used to determine the time-integrated spatial distribution and total energy of SBS and SRS independently.

*chow3@llnl.gov; phone 925-422-7615

The NBI scatter plates installed in 2009 and have degraded over time, especially as the fusion neutron and γ yields have increased. The NBI scatter plate assemblies were taken apart, and the Spectralon tested for material changes. The elemental composition and bonding were examined by FTIR, XPS and RBS; the surface morphology by SEM; and mechanical strength from tensile test specimens.

2. NBI Assembly Hardware

2.1 NBI Assembly Materials

An NBI scatter plate assembly nominally consists of six flat, rectilinear sub-assemblies with the Spectralon sandwiched between an Al base and 3.3 mm thick borosilicate glass cover. The glass protects the Spectralon from target debris and slightly attenuates the UV light. Spectralon is a high-purity polytetrafluoroethylene (PTFE) polymer that reflects wavelengths of light from UV to IR wavelengths in a near-Lambertian fashion.⁴ Plates of the material is pressed and sintered at 360C and then baked at 90C in a vacuum of 100 mTorr for 2 to 3 days by the supplier.⁵ The sub-assemblies are installed inside the NIF target chamber, as shown in Figure 1.

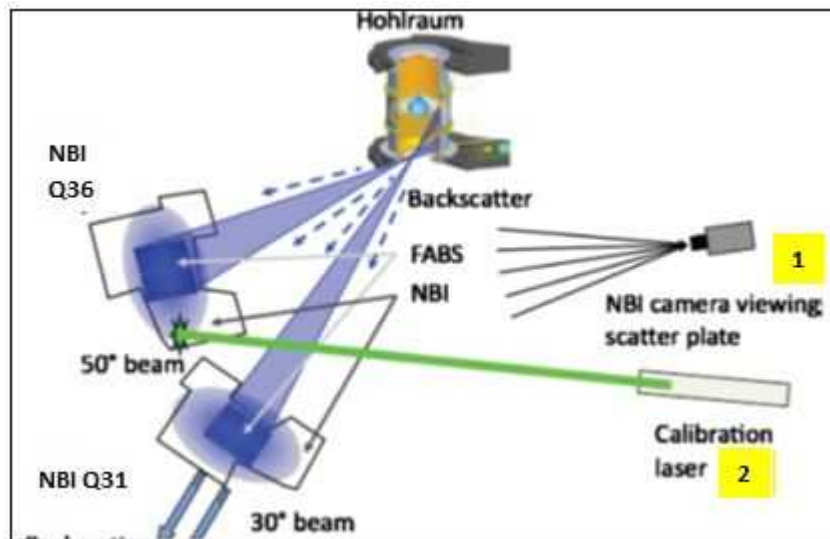


Figure 1 The backscatter system consists of (1) Instrument for viewing the NBI diagnostic at laser beam quads Q31 and Q36, and a (2) pulsed laser calibration instrument.

There are two NBI assemblies mounted on the inside wall of the NIF target chamber. Figures 2 are a top view sketch and photograph of an NBI assembly from the viewing camera. Each assembly is arranged around the apertures where a quad of NIF laser beams enters the target chamber. NBI Q31 is located at the beam quad 31B, near the south pole of the target chamber. NBI Q36 is located at the beam quad Q36B, slightly below the equator of the target chamber. NBI Q31 and NBI Q36 measure the backscatter contributions from beam entering the hohlraum at cones angles of 30° and 50°, respectively.

The picture in Figure 2b of NBI Q31 shows little visual evidence of shot-induced degradation. NBI Q31B had been in service for about 4 years and experienced a cumulative neutron and gamma radiation dose of 0.0384 Gy. It was not until the cumulative dose reach about 0.0826 Gy that reflectivity degradation was observed in various parts of the assembly.

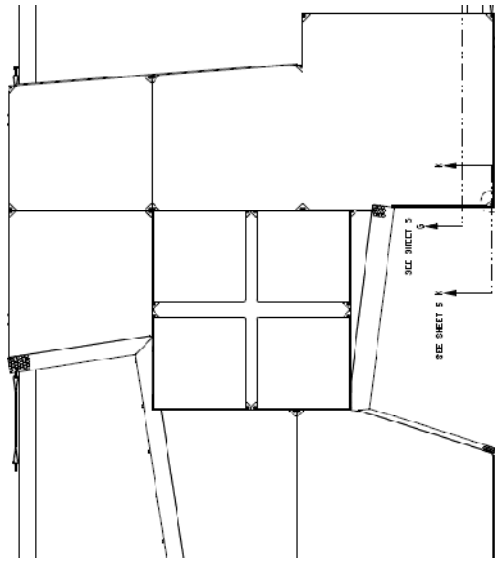


Figure 2a Top view sketch of an NBI Scatter plate assembly. There are 6 plates arranged around a quad of beams. These plates and the center cross are composed of Spectralon sandwiched between an Al base and cover glass. For scale, the length and width of the cross are 611 x 614 mm.

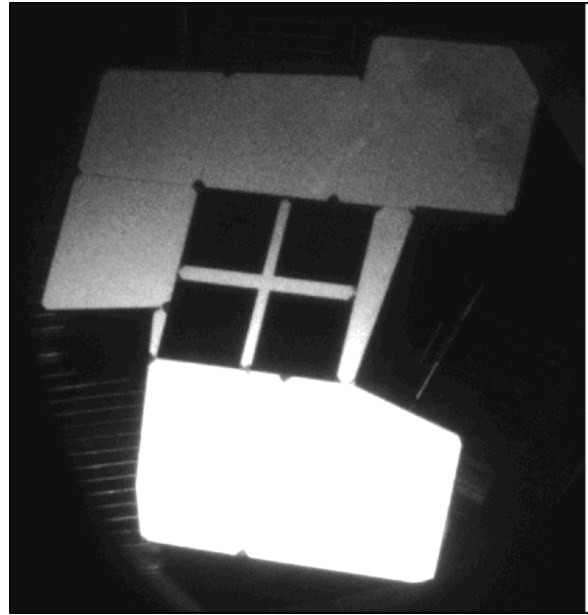


Figure 2b Image taken on June, 2011, of the NBI assembly on Beam Quad 31. Note the lack of defects although the assemblies have been irradiated with a cumulative dose of 0.0384 Gy, about 4 years of service in the target chamber.

2.2 Reflectivity Degradation

The close-up photographs of two NBI assemblies are shown in Figures 3. The NBI Q36 assembly, near the equator of the target chamber, was almost completely darkened by the time this study was initiated. Upon removal from the target chamber and disassembly, the top surface (facing the target) of the cover glass was metallized and pitted with target debris, but the underlying Spectralon was pristine in appearance (See Figure 4.)

The situation is reversed on the NBI Q31 assembly, located near the south pole of the target chamber. During the time frame when the localized reflectivity changes were tracked, the camera imaging system did not have sufficient resolution to determine if the defects were forming

1. on top of the cover glass from target debris and deposition
2. on or in the Spectralon, or
3. at the interface between the two layers, where possibly target debris penetrated the glass and was diffusing within the interface.

Upon removal from the target chamber and disassembly, the top surface of the cover glass was clean except for pitting from target debris. The bottom of the cover glass was smooth and there was no visual evidence of pits extending to the backside of the glass. The underlying Spectralon was the source of the reflectivity changes. The localized reflectivity changes appear as discolored, charred Spectralon.

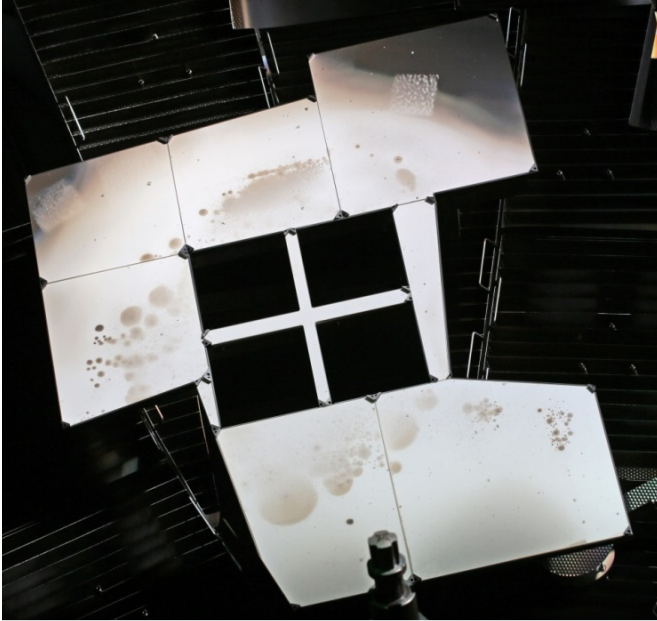


Figure 3a NBI Q31 assembly prior to removal on April, 2014. NBI Q31 is located near the south pole of the target chamber. Note the spatially localized reflectivity degradation of the Spectralon sub-assemblies.

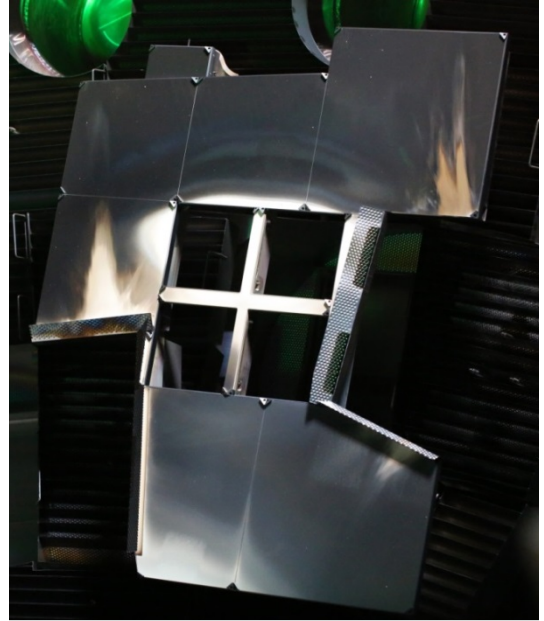


Figure 3b NBI Q36 assembly prior to removal on April, 2014. NBI Q36 is located near the equatorial level of the target chamber. Note the metallization of the cover glass.



Figure 4 Typical Spectralon and cover glass from a NBI Q36 sub-assembly. The Spectralon is pristine in appearance. The cover glass is metallized.

In Figures 5, the lower left NBI Q31 sub-assembly shows defect clusters and different regions of reflectance. A line was drawn across defect clusters that grew in a measurable manner. One of the defects is labeled as Defect #1. There are some defects that appeared to grow as rapidly but they eventually merged with other defects within the cluster.

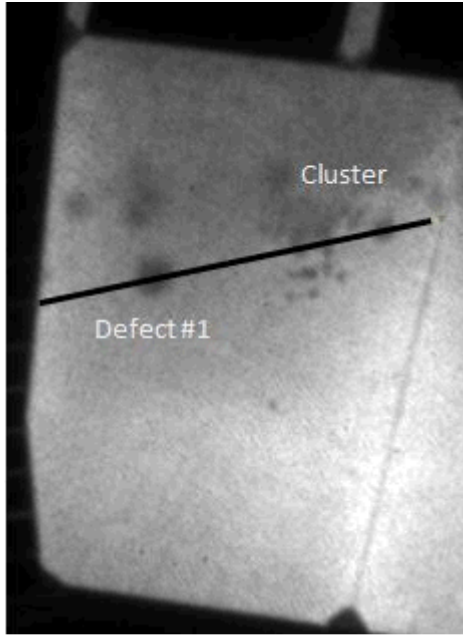


Figure 5a NBI Q31B defects with rapid growth are noted along the line drawn by software. Image taken April 2012.

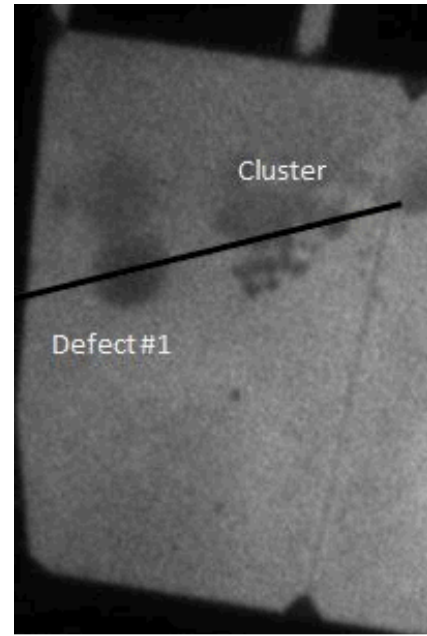


Figure 5b NBI Q31B defects merged together in the area labeled Cluster. Image taken November 2012.

3. Defect Analysis

3.1 Defect Growth Rate

The growth rate of Defect#1 was determined from 4 images taken on Jan, April, July and November of 2012. A 1Mp scientific camera⁶ captured the images using the illumination from the NIF chamber camera view imaging system. The ImageJ software⁷ was used to measure the intensity across the defect from which the diameter was measured at FWHM. The pixel-to-length conversion was calculated from the nearest aperture edge of the quad opening. The normalized intensity profiles from Defect #1 are shown in Figure 6 for the given dates. The growth rate was calculated to be 0.212 mm/day.

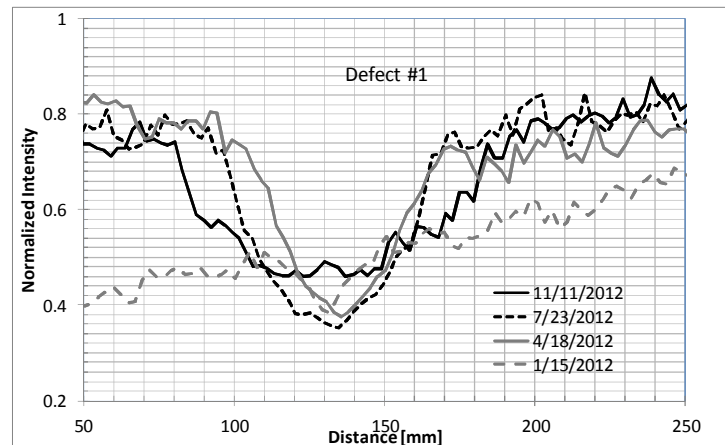


Figure 6 Defect #1 line-outs of its normalized intensities

The exposure of the NBI assemblies to energetic particles and photons that could create defects depends more on the shot rate than a time-duration. One of the NIF metrics application archives the actual neutron and α yields for every Deuterium-Tritium D-T and D-D fusion reaction on a per shot basis. The α yields are not considered any further since these particles are stopped by the cover glass from reaching the Spectralon. From the neutron yield database and the

physics model of the radiation doses around the NIF target chamber for a 20 MJ target shot, one can determine the dose of 14.1 MeV neutrons and energetic γ radiation for any given shot at the NBI assembly position,

$$N_{\gamma Z} = N_{\gamma 20} * [N_Z / N_{20}], \quad (1)$$

where N_{γ} is the neutron dose plus gamma dose in Gy units, N is the neutron yield, the subscript 20 is 20 MJ of energy from the target, the subscript Z designates the shot of interest.⁸ The growth of the defects, at FWHM, was plotted against the cumulative N_{γ} dose, ΣN_{γ} , that the NBI assemblies had received at the dates the images were collected. The defect growth rate is 900 mm/Gy with a high correlation a linear fit. The purpose of this analysis was to estimate the remaining service life of the current and future NBI assemblies.

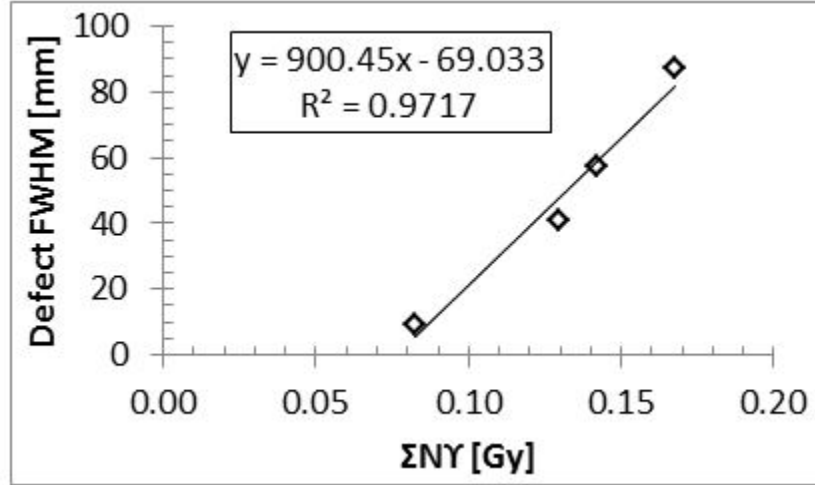


Figure 7 Defect growth as a function of cumulative neutron and gamma radiation dosage, ΣN_{γ} . Growth rate is 900 mm/Gy.

3.2 Materials Characterization of Spectralon and Discussion

Spectralon plates extracted from the NIF target chamber in April of 2014 had been irradiated with a $\Sigma N_{\gamma} = 0.74$ Gy. The lower two Spectralon plates from NBI Q31 were selected for multiple materials analysis. The Spectralon plates were decontaminated by washing with hot water, wiped down with solvents, and allowed to decay until the radioactive levels were below that of levels found in the general public. These two plates were representative of the discoloration range observed in the other NBI Q31 plates, from a pristine white to brown to black, as represented in Figures 8. All non-white colorations were on the surface of the Spectralon facing target chamber center, whereas none of the discolorations extended to the backside of the Spectralon. One cm diameter core samples for chemical analysis and tensile samples for mechanical testing were machined, without lubrication, from these plates in areas that had a no visible discoloration, a brown color, a black color and from a Spectralon sample that was purchased in the same lot but never installed in target chamber. The sample designations are White-X, Brown-X, Black-X and Non-Irradiated, respectively, where X = 1 for samples machined from the left plate and X = 2 for samples machined from the right plate. The cover glass was broken during the target chamber extraction on the plate from the lower right assembly. The purpose of the red tape shown Figure 8b was to keep the glass in-place during the extraction procedure.



Figure 8a Spectralon samples (Label X = 1) were cored from the NBI Q31 sub-assembly, lower left plate, for RBS and XPS analysis.

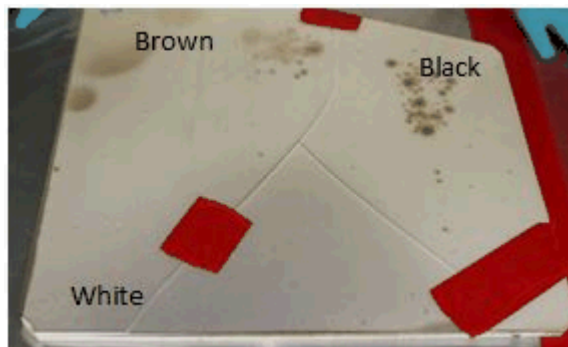


Figure 8b Spectralon samples (Label X = 2) were machined from the NBI Q31 sub-assembly, lower right plate for FTIR, SEM and mechanical characterization. Note the cover glass was broken during the target chamber extraction.

3.2.1 Rutherford Backscattering Spectrometry (RBS)

RBS was conducted on samples Non-Irradiated-1, White-1, Brown-1, and Black-1.⁹ The RBS spectra were acquired at a backscattering angle of 160° and an appropriate grazing angle with the sample oriented perpendicular to the incident ion beam. The sample is rotated or tilted with a small angle to present a random geometry to the incident beam to avoid channeling in both the film and the substrate. The other RBS parameters are He^{++} ion beam energy of 2.275 MeV, grazing detector angle of about 100° , and a CC RR analysis mode. Spectra are fit by applying a theoretical layer model and iteratively adjusting the concentrations and thickness until good agreement is found between the theoretical and the experimental spectra. Table 1 list the atomic % of C and F for the four samples. There is no statistical difference in the C and F atomic concentrations among the samples. The top surfaces of the samples, even the Non-irradiated control sample may have been heavily contaminated with hydrocarbons since the atomic C/F ratio is between 0.8 to 0.9 instead of the stoichiometric PTFE 0.5 ratio.¹⁰ Other reasons for a non-stoichiometric ratio is that the samples may charging or there is preferential ion-induced F-loss.¹¹

Table 1 RBS Analysis shows no statistically significant differences in the C/F atomic ratio between the samples to an estimated $3.3 \mu\text{m}$ depth.

Sample	C \pm 2 at %	F \pm 2 at %	C/F Ratio
Non-Irradiated	47.0	53.0	0.887
White-1	44.5	55.5	0.802
Brown-1	46.5	54.5	0.853
Black-1	47.5	52.5	0.905

3.2.2 FTIR

The Spectralon sample spectra were obtained using a Harrick Split Pea attenuated total reflectance (ATR) feature, equipped with a silicon crystal, mounted in a Perkin Elmer Spectrum GX FTIR spectrophotometer. The wavelength range scanned was 2.5 to $25 \mu\text{m}$ (4000 to 400cm^{-1} wavenumbers). The spectra from all the “-2” samples were essentially identical (Figures 9a). The slight transmission variations are possibly caused by the different surface roughness between the samples. The probe depth of the evanescent wave protrudes from the ATR crystal into the sample about 0.5 to $5 \mu\text{m}$. The FTIR library spectra routine identified each of the White-2, Brown-2 and Black-2 samples as PTFE (Figure 9b).

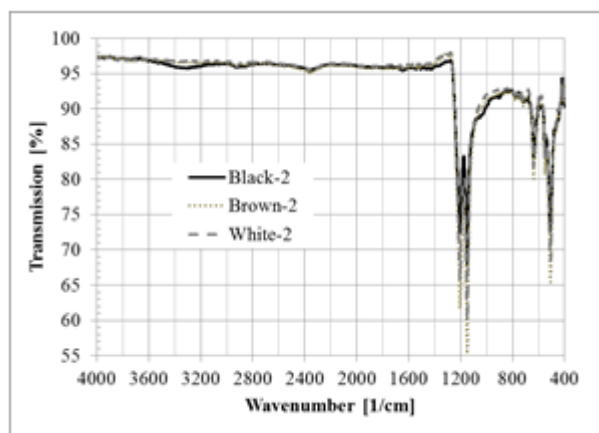


Figure 9a The samples are essentially identical per FTIR analysis.

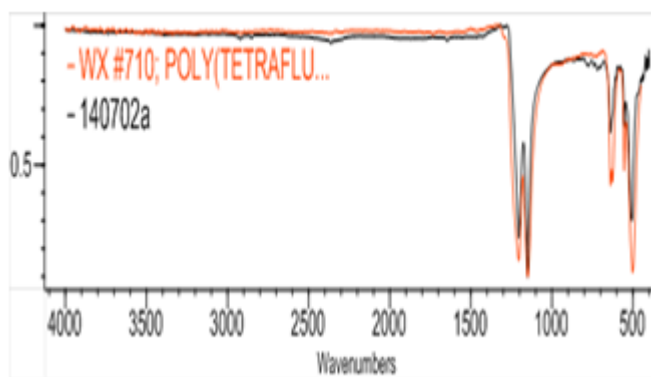


Figure 9b FTIR Spectra from the White-2 sample overlaid to that of PTFE from the FTIR spectra library.

3.2.3 XPS analysis

XPS was used because it is a more surface sensitive technique compared the RBS and FTIR techniques above. XPS was conducted on White-1, Brown-1 and Black-1 samples.¹² XPS data was quantified using relative sensitivity factors and a model that assumes a homogeneous layer. The analysis volume is the product of the analysis area (spot size or aperture size) and the depth of information. Photoelectrons are generated within the X-ray penetration depth (typically many microns), but only the photoelectrons within the top three photoelectron escape depths are detected. Escape depths are on the order of 15-35 Å, which leads to an analysis depth of ~50-100 Å. Typically, 95% of the signal originates from within this depth. The XPS analytical parameters are given in Table 2.

Table 2 XPS analytical parameters

Instrument	PHI Quantum 2000
X-ray Source	Monochromatic Al k 1486.6 eV
Acceptance Angle	$\pm 23^\circ$
Take-off Angle	45°
Analysis Area	1400 μm x 300 μm
Charge Correction	C1s 284.8 eV

The XPS analysis shows that the less dis-colored the surface, the more it resembles un-irradiated Spectralon. In Table 2, the White-1 sample has an atomic C/F ratio of 0.71, comparable to the ratio of 0.80 determined from the RBS analysis on the same sample. As the discoloration darkens, there is less F with more C, N and O detected. The XPS atomic C/F ratios are 1.02 and 2.17 in the Brown-1 and Black-1 samples, respectively.

Table 3 Atomic concentrations [%] at the surfaces of the Spectralon samples; and the C/F ratios.

Sample	C	N	O	F	Na	Si	C/F
White-1	40.3	0.4	2.2	56.7	<0.1	0.4	0.71
Brown-1	47.8	0.5	4.7	46.7	0.1	0.2	1.02
Black-1	61.7	1.0	8.7	28.4	0.2	0.1	2.17

Table 4 and Figure 10 show the relative surface concentrations of likely CF, organic, and N-molecular species. As the discoloration darkens, there is a significant decrease of CF₂ detected and an increase of the other species. The decreasing CF₂ surface concentration can occur either by or all of re-formulated species, impurity layers that mask the underlying matrix, and/or the F-loss. There are reports [Harling et al, Ryan et al] of neutron and γ radiation breaking the C-F bond with subsequent C=O bond formations from the CF₂ molecules. In the NIF chamber environment, the broken bonds from the surface CF₂ molecules possibly leaves the C to bond to other species typically found in a high vacuum, such as N₂ and H₂O, and CF_x molecules. The formation of these species at the surface may mask the undamaged CF₂ from XPS detection.

Impurities from the de-contamination process may have contributed to the XPS observations. Spectralon is porous and was noted to absorb the solvents used during the decontamination procedure. However, there was no detection from RBS and the FTIR analysis indicating the presence of such solvents. XPS detects the formation of CF_x , organics and N-molecular species that increase as the discoloration darkens.

The decreasing F surface concentration may be caused by F-loss. The diagnostic group that performs the radioactive gas analysis for NIF shots reports large bursts of F_2 during the shot.¹³ However, the species is activated F_2 atoms. The concentration of un-activated F_2 that would be expected from the Spectralon has not yet been observed via this gas analysis diagnostic. One possibility may that the free F atoms are captured by the glass cover and cannot diffuse out to the gas probes.

Table 4 Carbon Chemical States in % of total C

Sample	C-C, C-H	C-O, C-N	C=O, C-CF _x	O-C=O, CF	CO ₃ , CF-CF _x	CF ₂
White-1	22	6	2	2	1	67
Brown-1	32	10	5	4	2	47
Black-1	50	15	7	5	2	20

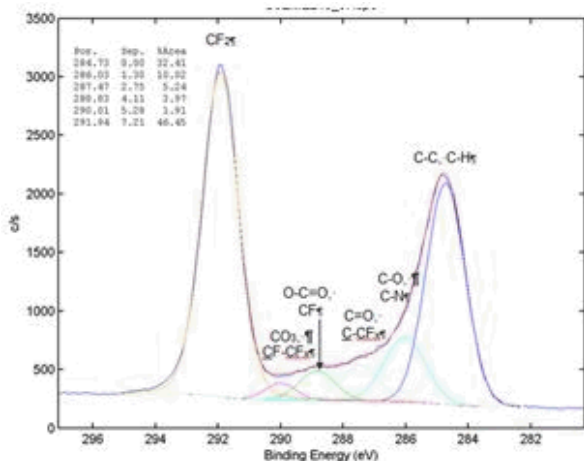


Figure 10a XPS spectra from sample White-1. Note the relatively high counts at the CF_2 binding energy at 292 eV and low counts of C-C and C-H molecules at 285 eV.

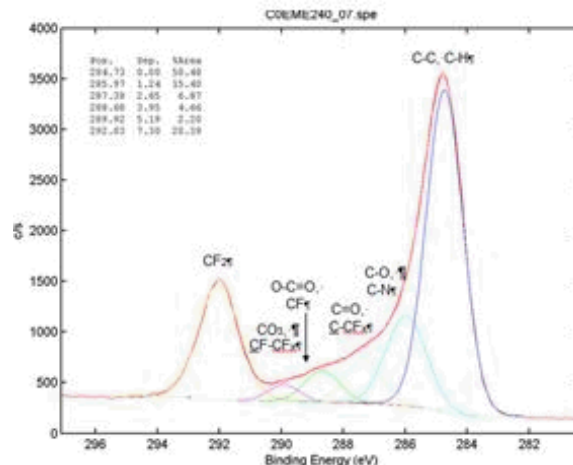
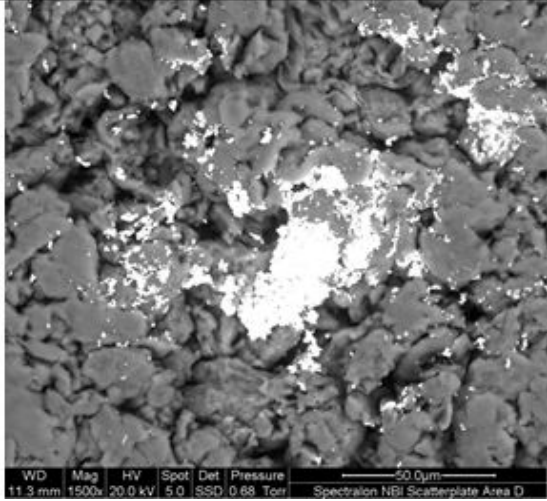
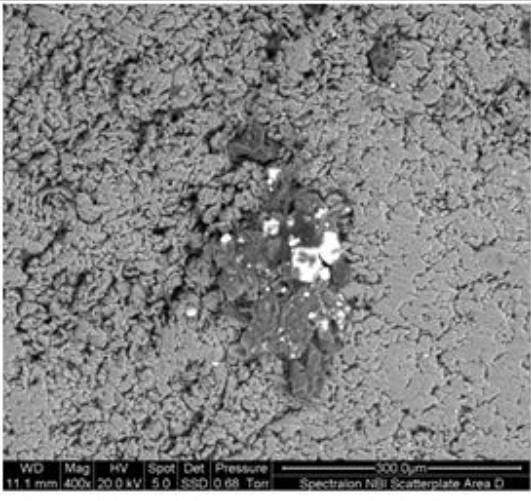
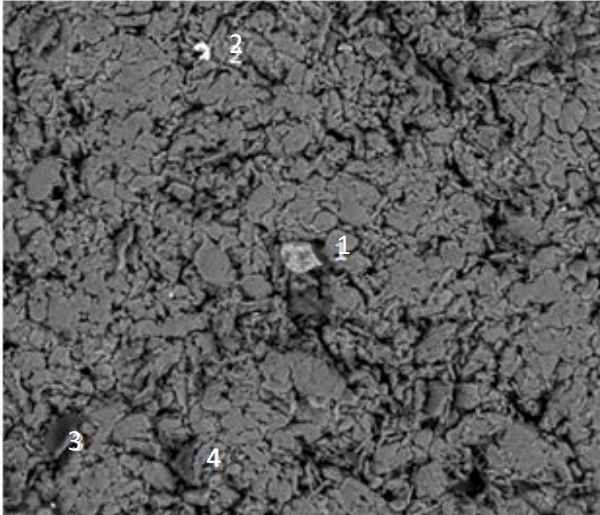


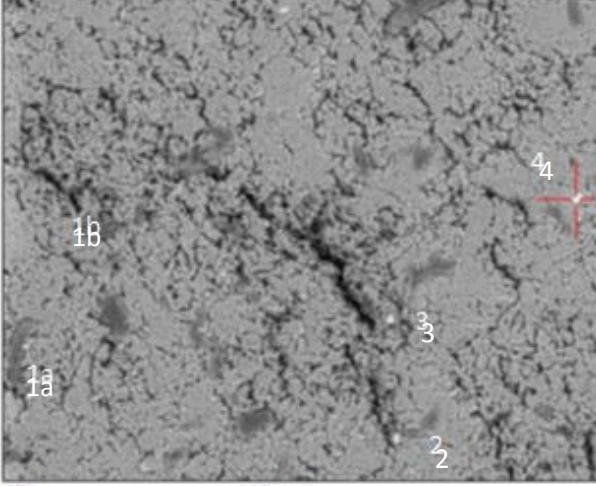
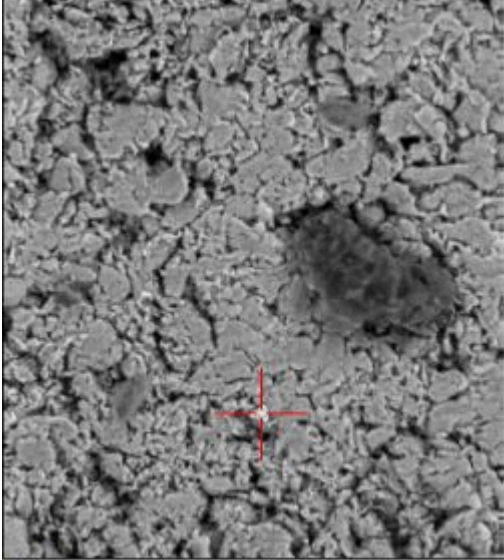
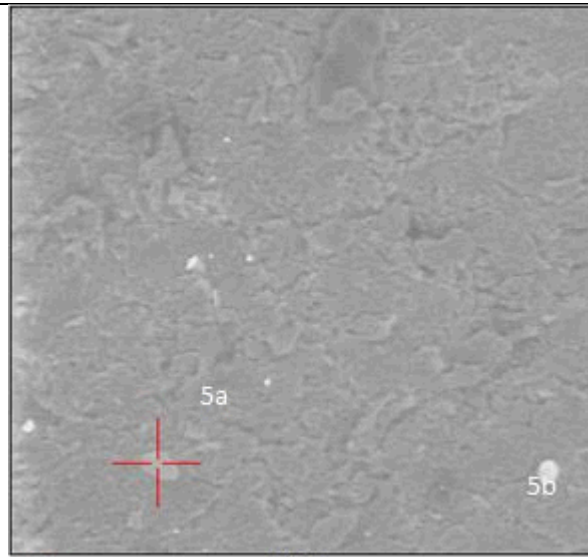
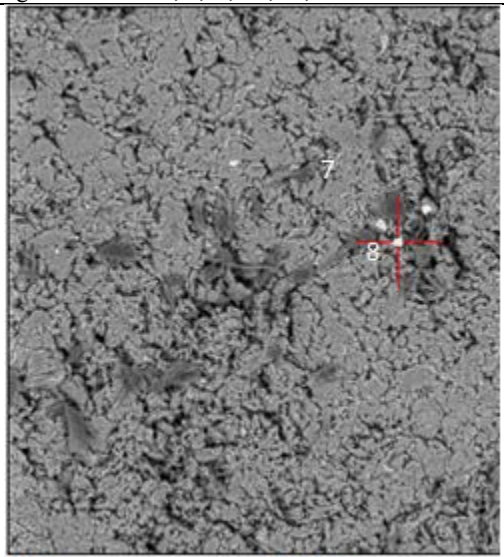
Figure 10a XPS spectra from sample Black-1. Note the relatively low counts at the CF_2 binding energy at 292 eV and high counts of C-C and C-H molecules at 285 eV.

3.3.4 Energy Dispersive Spectroscopy and SEM analysis

SEM and Energy dispersive spectroscopy (EDS) analysis was performed on samples White-2, Brown-2 and Black-2. The EDS probe of the surface without any protrusions or notable features is composed of only C and F atoms. EDS was conducted on surface features that appeared frequently in the SEM images. The elements presented by the EDS may be attributed to the mineral oxides of borosilicate glass.¹⁴ There was a possibility that broken glass shards were imbedded in the Spectralon during the extraction from the target chamber and de-contamination of the NBI sub-assemblies (Figure 8b). There are features on Brown-2 and Black-2 samples which appear dark in the SEM images. These features only contain C, F and O elements according to the EDS analysis. This is consistent with the XPS analysis that there a decrease of F detected with an increase in C-O forming molecules. The EDS analysis did not find any N containing particles in contrast to the XPS analysis.

Table 5 SEM images and EDS results. The EDS results indicated that broken borosilicate glass was imbedded onto the Spectralon.

ID		
White2	 <p data-bbox="358 835 730 863">Bright, Round particle: C, F, O, S, Ti</p>	 <p data-bbox="868 835 1341 863">Bright, Cubic particle: C, F, O, Na, Al, Si, Cl, K</p>
Brown2	 <p data-bbox="240 1430 630 1535"> Particle 1: C, F, O, Na, Al, Si, Cl, K, Ca Particle 2: C, F, O Na, Cl, K Particle 3: C, F, O Particle 4: C, F, O, Na, S, Cl, K, Ca </p>	<p data-bbox="1084 1167 1187 1194">No Image</p>

Black2	 <p>SE1 100µm</p> <p>Dark Particles 1a, 1b: C, F, O Bright Particle 2: C, F, O, Na, Mg, Al, Si, K Bright Particle 3: C, F, O, Mg, Al, Si, Ca Bright Particle 4: C, F, O, Zn</p>	 <p>SE1 50µm</p> <p>Bright Particle 6: C, F, O, Na, Al, Si</p>
Black2	 <p>SE1 100µm</p> <p>Bright Particles 5a and 5b: C, F, O, Al</p>	 <p>SE1 100µm</p> <p>Bright Particle 7: C, F, O, Na, Mg, Ca Bright Particle 8: C, F, O, Si, Fe</p>

3.3.5 Mechanical properties

The mechanical properties were determined according the ASTM D638 standards.¹⁵ Five Type V dog-bone samples were prepared from the NBI Q31 plate mentioned above as well as from Spectralon that was not installed in the target chamber.

The mechanical data shows, in Figures 10a and b, that Brown-2 samples had the highest load and elongation values, followed by Black-2 samples, and lastly the White-2 samples. In this case, color change was not an indicator of any degradation in the mechanical properties. It is also believed that the variation in results from the various specimen groupings is most likely due to processing the material since the material is porous as can be seen in the SEM images. Small changes in cell structure can have large impacts on mechanical properties. This is further supported by the results

from samples cut from the center of the Spectralon sheet, where these samples consistently produced slightly lower values when compared to specimens that had only one outer surface un-machined.¹⁶

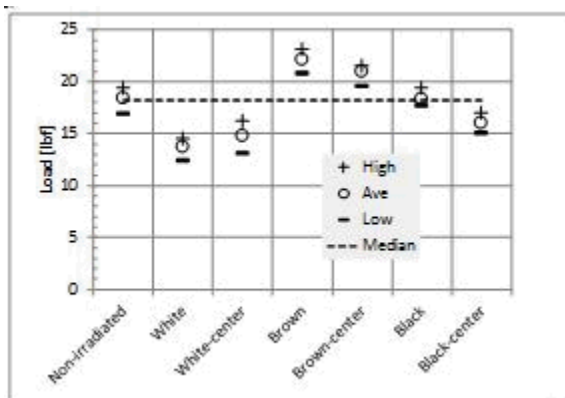


Figure 10a Tensile load averages

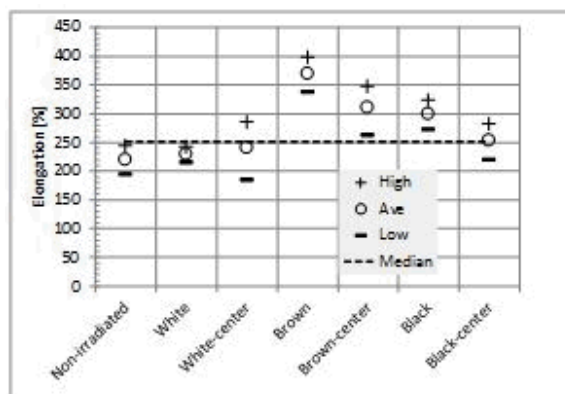


Figure 10b Elongation averages

4. Discussion and Conclusion

RBS, FTIR, and mechanical tests could not differentiate between irradiated and non-irradiated samples of Spectralon. These measurements were performed on samples in service on the NBI diagnostic assemblies, inside the NIF target chamber where they were irradiated with a cumulative combined neutron and γ dose of 0.74 Gy. Bulk Spectralon did not degrade according to these measurement techniques.

However, the Spectralon surfaces develop discoloration from a pristine white to brown to black in various areas of the plates. The reflectivity changes were noticed after the Spectralon was irradiated with a combined cumulative neutron and γ dose of 0.0384 Gy. Stiegman et al.¹⁰ report yellow color changes of Spectralon when irradiated with intense ultra-violet light from a Xe-arc lamp while in vacuum. They attributed the discoloration to a photo-chemical mechanism whereby volatile impurities diffuse to the surface, UV illumination breaks down the impurities, and reaction products form an organic layer at the surface. Their proposed solution to avoid discoloration was to remove the volatile organic contamination by vacuum-baking the Spectralon. The photo-chemical mechanism may not be the cause of the reflectance for two reasons. First, the NBI Spectralon was vacuum-baked. Second, the discoloration on the NBI Spectralon was brown and black instead of yellow.

A photo-thermal mechanism is more consistent with observations and analysis herein. The NBI Q36 Spectralon looked pristine because the metallized glass sufficiently attenuated the UV backscatter light from reaching the Spectralon. The NBI Q31 Spectralon was exposed to backscatter light at 350 nm of pulse durations on the order of nano-seconds which chars PTFE.¹⁷ The charring appears as spatially localized black spots and was attributed to intentional doping of the PTFE with absorbing impurities. Also, the charring was confined to the surface exposed to UV light.¹⁸ Other studies about UV laser ablation of PTFE showed de-fluorination¹⁹ and chemical bonds forming with ambient vapor species at the surface.¹⁸ There may have been unintentional absorbing impurities trapped along the seam between two Spectralon plates. Figure 11 shows the defects aligned along the seam, which would have a high probability of impurities concentrated at the interface. The NBI Spectralon may need a longer vacuum-bake time or the material was re-contaminated during the storage, assembly, or installation of the NBI structure in the target chamber.

Possible options to purify the Spectralon, especially at the surface illuminated by the UV light, may be to deposit high purity Spectralon onto the backside of the cover glass. The coated glass would be backed up with a thick Spectralon plate to maintain the optical scattering properties.¹⁹ A Spectralon coated cover-glass would have the extra advantage of protecting the illuminated surface from contamination due to handling and installation. Painting a high purity solution of Spectralon on the surface has been attempted but this application process leaves streak marks of irregular reflectances. LPCVP,²¹ thermal evaporation,^{22,23} and RF sputtering²⁴ to create PTFE-like films has been demonstrated. However further study is needed to verify that the Spectralon coatings are purer than the bulk-fabricated Spectralon and the optical properties are acceptable for the NBI diagnostic.



Figure 11 Defects preferentially aligned to a seam in the Spectralon plate. The seam appears to seed defect growth. Defects are prevalent on the right section of the plate and not the left section.

5. Acknowledgements

Richard Meissner provided the FTIR analysis reported in Figure 9. Sharon Torres provided the for SEM analysis reported in Table 5. The authors would like to thank William H. Gourdin for providing support for the mechanical measurements and for reviewing the manuscript.

6. Auspices

Lawrence Livermore National Laboratory is operated by Lawrence Livermore National Security, LLC, for the U.S. Department of Energy, National Nuclear Security Administration under Contract DE-AC52-07NA27344.

7. References

- [1] Van Wonerghem, B. M., Brereton, S. J., Burr, R. F., Folta, P., Hardy, D. L., Jize, N. N., Keane, C. J., Kohut, T. R., Land, T. A., and Merritt, B. T., "Operations on the National Ignition Facility", LLNL-JRNL-772095, to be published in Fusion Science and Technology.
- [2] Moody, J. D., Datte, P., Krauter, K., Bond, E., Michel, P. A., Glenzer, S. H., Divol, L., Niemann, C., Suter, L., Meezan, N., MacGowan, B. J., Hibbard, R., London, R., Kilkenny, J., Wallace, R., Kline, J. L., Knittel, K., Frieders, G., Golick, B., Ross, G., Widmann, K., Jackson, J., Vernon, S., and Clancy, T., "Backscatter measurements for NIF ignition targets", Rev Sci Instru 81(10D921), 1-6 (2010).
- [3] Ralph, J. and Hibbard, R., private communication, Nov. 2014.
- [4] Bruegge, C. J., Stiegman, A. E., Rainen, R. A., and Springsteen, A. W., "Use of Spectralon as a diffuse reflectance standard for in-flight calibration of earth-orbiting sensors," Opt Eng 32(4), 805-814 (April 1993).
- [5] Labsphere, Inc., 231 Shaker Street, North Sutton, NH 03260, E-MAIL: labsphere@labsphere.com, <http://www.labsphere.com>
- [6] Pi-Max Model 7467-0022, Princeton Instruments, 3660 Quakerbridge Rd, Trenton, NJ 08619 USA.
- [7] NIH website: <https://www.imagej.nih.gov/ij>
- [8] Khater, H., "Neutron and Gamma Background Maps for a 20 MJ Shot," LLNL internal distribution, Dec. 9, 2011
- [9] EAG Report C0EME240AT, Evans Analytical Group, 810 Kifer Road, Sunnyvale, CA 94086.

- [10] Stiegman, A. E., Bruegge, C. J., and Springsteen, A. W., "Ultraviolet stability and contamination analysis of Spectralon diffuse reflectance material", *Opt Eng* 32(4), 799-804 (April 1993).
- [11] Kucheyev, Sergei O., private communications, April 2015
- [12] EAG Report C0EME240XP, Evans Analytical Group, 810 Kifer Road, Sunnyvale, CA 94086.
- [13] Jedlovec, D., private communication, 2015.
- [14] Fire Retardancy of Polymeric Materials, 2nd Edition, 2010, Section 9.2.8.1, Borosilicate, Borosilicate Glass, and Frits, page 228.
- [15] ASTM D638-10, Standard Test Method for Tensile Properties of Plastics.
- [16] Jensen, W., Gourdin, W., and Pearson, M., Analysis of Spectralon® NBI Scatter Plate Removed From NIF Target Chamber, NIF Report # NIF0175966-AA (August 2014).
- [17] Krüper, S. & Stuke, M., "Ablation of PTFE with femtosecond UV excimer laser pulses," *Appl Phys Lett* 54(1989) 4
- [18] Ferry, I., Vigier, G., Alexander-Katz, R., Garapon, C., "Interaction between UV Radiation and filled PTFE I. Degradation Processes," *J Polymer Sci* 36 2051-2067 (1998)
- [19] Chtaib, M., Roberfroid, E.M., Novis, Y., Pireaux, J.J., Caudano, R., Lutgen, P., and Feyder, G., "Polymer surface reactivity enhancement by UV ArF laser irradiation: An XPS study of polytetrafluoroethylene and polyethyleneterephthalate UV treated surfaces," *JVST A7* 3233-3237 (1989).
- [21] Labsphere website: <http://www.labsphere.com/uploads/datasheets/6080-product-sheet.pdf>, Section 2.4
- [22] Rastogia, A.C. & Desu, S.B., "Structural development and electronic properties of hot filament low pressure chemical vapor deposited fluorocarbon polymer films," *J. Mater. Res.* 21, 242-254 (Jan 2006)
- [22] Nason, T.C., Moore, J.A., and Lu, T.-M., "Deposition of amorphous fluoropolymer thin films by thermolysis of Teflon amorphous fluoropolymer," *App Phys Lett* 60, 1866-1868(1992)
- [32] Chow, R., Loomis, G. E., Ward, R. L., "Optical Multilayer films based on an amorphous fluoropolymer", *JVST A14* 63-68 (1996).
- [24] Biederman, H., "The properties of films prepared by the rf sputtering of PTFE and plasma polymerization of some Freons," *Vacuum* 31, 285-289(1981)